ORIGINAL

Visible dynamic changes in the mechanism of water evaporation surface formation during wood drying

Xiang Chi[1,2] · Sai Tang[1] · Xiaoxue Song[1] · Ren Zechun[1] · Gangping Han[3] · Wanli Cheng[1] · Stavros Avramidis[2]

Abstract

Internal moisture distribution seriously affects timber shrinkage relations during drying, and it is also an essential parameter for testing the validity of a three-dimensional heat and mass transfer model. Here, we present an experimental study of 3D changes in moisture content at different stages during constant temperature and humidity drying of two wood species, covering visible moisture movement evaporation surface, 2D and 3D moisture variations, moisture values in the dry and wet zones, and color changes. We show that the evaporating surface was a wet front, its influence on the wood 3D structure is in the tangential > radial > longitudinal direction, and the color difference ranges from 10.6 to 17.6 when the wet front is present. Moisture values for poplar and pine at the disappearance of the wet front ranged from 14.2–19.7% to 20.4–22.5%, respectively. In mass transfer during wood drying, wood dimensional simplification and homogenization in the drying model should not be used, and the moisture content in each wood thickness layer should be evaluated in a diversified manner.

✉ Wanli Cheng
  nefucwl@nefu.edu.cn

✉ Stavros Avramidis
  stavros.avramidis@ubc.ca

1   College of Material Science and Engineering, Northeast Forestry University, Harbin 150040, China

2   Department of Wood Science, University of British Columbia, Vancouver, BC V6T 1Z4, Canada

3   Ministry of Education, Key Laboratory of Bio-Based Material Science and Technology, Northeast Forestry University, Harbin 150040, China

Introduction

Wood is a renewable biomaterial widely used in construction because of its high strength-to-weight ratio (He et al. 2020; Lu et al. 2022; Gan et al. 2021; Guan et al. 2018; Chen et al. 2020). Wood moisture content (M) and distribution are essential factors in wood drying, processing, and storage. To ensure optimum quality and performance in service, freshly milled timbers from logs must be dried appropriately quickly with minimum degradation and energy use.

M changes during drying are usually described by simplifying the wood's geometry and finding its overall diffusion coefficient using traditional semi-empirical mass transfer theory (Droin-Josserand et al.1989; Avramidis et al.1994; Chiniforush et al. 2019; Gambarelli and Ožbolt 2021). In contrast, Turner et al. (2011) considered that wood is a highly heterogeneous, fractal medium, and the conventional diffusion equation may not adequately describe the movement of water in the internal pore network because water diffusion is anomalous (non-Fickian) and, therefore, used a water potential with Laplace raised to a fractional index to define the fractal space operator. A coupled anomalous transport model for temperature (T) and M is then derived to simulate water adsorption in the wood's cell walls.

However, the changes in M distribution in the internal spatial structure of a drying timber are influenced by the synergy of multiple physical fields. Adamski and Pakowski (2013), Redman et al. (2018), Zhao and Cai (2017), and He et al. (2019) used numerical modeling and multi-physics field coupling, plus the conservation of momentum, mass, and energy combined with the space operator to study the heat and mass transfer and mechanical properties during wood drying. The static solution method is used to visualize the stratified temperature scatter and stratified M scatter over the thickness of the wood at a particular time using point and line plots and contour plots. Except for the weighing method (Chi et al. 2020; Lingayat et al. 2020), the other M determining techniques need to consider the effect of the complex calibration techniques and parameter solutions. The error range for wood M measurements above the fiber saturation point (M_{fsp}) is between 3 and 50% (Fredriksson et al. 2021; Kandala et al. 2016; Chetpattana-nondh et al. 2017; Pan et al. 2016; Oliveira et al. 2005; Oh et al. 2020; Arends et al. 2018a, b; Cai et al. 2020; Mikac et al. 2018; Li et al. 2013; Watanabe et al. 2008; Gilania et al. 2014; Purba et al. 2020). So, further development of their accuracy and 3D imaging capabilities is needed if they are to be used to detect internal M profiles in wood drying.

Hao et al. (2020) used a numerical model to study the migration process of the moisture moving evaporation surface (wet front) along the timber thickness, considering the dry and wet zones of the wood as bounded by the M_{fsp} and predicted the change of the moving evaporation surface by predicting the M over 1/2 and 1/4 of the wood thickness during the drying process. Chi et al. (2022) referred to a "wet line," which was thought to be caused by the diffusion of non-homogeneous M over the thickness of the wood during drying (Avramidis et al. 1994). Since wood is a three-dimensional structure, the moisture distributions in

the three-dimensional direction are not simply variable either. Therefore, the concept of M evaporation surface can be borrowed, and a suitable detection method can be used to determine the water evaporation domain.

In this study, the M on the three-dimensional timber spatial scale and color values of the dry and wet zones during drying were determined to investigate the relationship between the visible M profiles and color as well as the mechanism for the appearance and disappearance of M profiles. The study may allow the quick identification of M profiles and provide a theoretical basis for improving the 3D model for heat and mass transfer during drying.

Materials and methods

Sample preparation and experimental procedure

Poplar (*Populus* L.) and camphor pine (*Pinus sylvestris* var. *mongholica* Litv.) are two common tree species growing in northeastern China. Timber from Harbin, containing pith, with length–width–thickness dimensions of 3600 mm×free width (10–13 mm)×50 mm and initial $M > 70\%$, was obtained fresh from a local sawmill.

To minimize the effect of wood variability, a whole piece of timber was selected for each experiment, and after cutting off 200 mm from each end, the remaining part was equally divided into six sections (experimental boards) and 10-mm sections of each end for the determination of the initial moisture content (M_i) as shown in Fig. 1. Then, the average M_i for each board was calculated from the six sections.

As one experimental board can only be dissected once at a specific M, six experimental boards are required to determine the moisture distribution on the
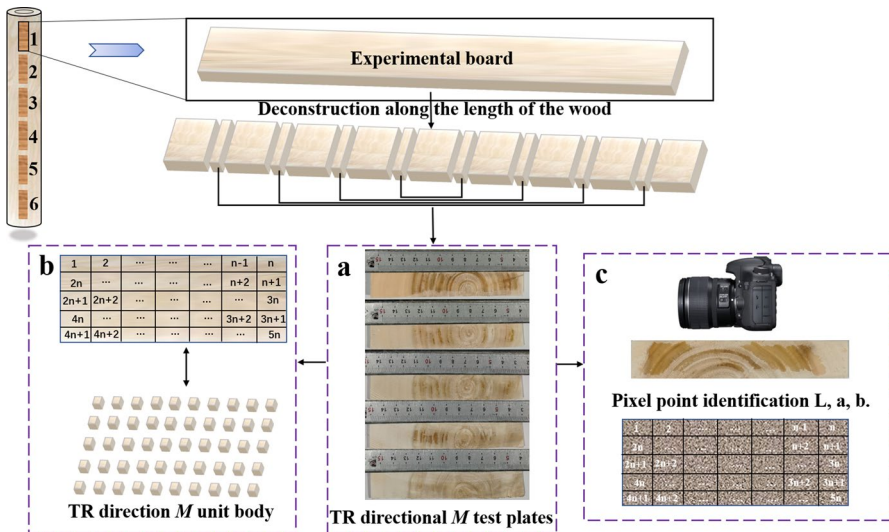

Fig. 1 Experimental flowchart

three-dimensional structure of the wood for six specific M conditions. So, six boards for each group of experiments, when the average moisture content ($\overline{M}$) for one sawn-off board during drying of poplar and pine was 60%, 50%, 40%, 30%, 20%, and 10%, which were recorded as Y-MC-60, Y-MC-50, Y-MC-40, Y-MC-30, Y-MC-20, and Y-MC-10 and S-MC-60, S-MC-50, S-MC-40, S-MC-30, S-MC-20, and S-MC-10, respectively.

Only the mass transfer behavior of wood was studied during drying, and the experimental boards of green poplar and camphor pine wood were dried at 60 °C and 60% relative humidity (H), respectively. Six marked experimental boards to be sawn at six different M levels were placed uniformly in the constant temperature and humidity chamber. When the M of the experimental boards reached the corresponding preset M stage, they were removed for three-dimensional dissection. As shown in Fig. 1, firstly, they were divided into eight equal parts in the longitudinal direction and sawn into eight M test pieces (MTPS) of 10-mm thickness each. Secondly, along the T–R direction of each MTP, the grid was gridded by 10×10 mm in length and width, using a ball pen to draw the grid and mark the serial number of each cell to make it recognizable after sawing.

Before sawing the small wooden block units, a non-contact optical system was used to take rapid images of each of the eight MTPs, which were used as the basis for color analysis in subsequent experiments. After the images were obtained, they were sawn into small blocks according to the cell dimensions of the grid, as shown in Fig. 1b. The small wooden blocks were quickly placed in sealed bags, weighed individually using a balance with an accuracy of 0.001 g, weighed and placed in an oven at 102 ± 0.5 °C, and baked until absolutely dry. This process was repeated one by one for each group of six experiment boards to be sawn until the drying experiment was completed when the board with a M of 10% had been sawn. A total of 2880 small wood block units were sawn in each set of experiments. The above experimental procedure was identical for the two wood species. The experiment was repeated twice for each wood species. A total of 11,520 small wooden block units were sawn for this experiment.

Three-dimensional imaging of wood moisture distributions

Steps of 3D imaging of wood moisture distributions: Each wood species experimental board was placed along the same longitudinal direction, with the starting point on the left side as the Cartesian coordinate (0; 0; 0) starting point. The spatial position of the deconstructed wood small unitary (L_i, R_i, and T_i) was recorded when $\overline{M}$ was 10%, 20%, 30%, 40%, 50%, and 60%, and its M was determined, and its 3D spatial position and M as four-dimensional data values (L_i, R_i, T_i, and M_i) were obtained, and the dataset was converted into a matrix using Origin 2021 software. The 3D color-mapped surfaces module of the software was used to create a 3D M cloud map to image the wood 3D moisture distributions on various $\overline{M}$ stages (see "Visible dynamic changes in 3D distribution of wood moisture during drying" section). During the drying process, this diagram presents the moisture distribution on the 3D structure of the wood in its spatial position. Where the longitudinal direction, radial

direction, and tangential direction represent the fiber, axis, and tangential direction of the wood, and *i* is the label of each small wood unit.

Gloss and color changes of two tree species at various M

During the drying experiment, the high magnification camera can record the color of each MTP pixel point on different *M*, allowing more accurate quantification of the color of the wet front. It is, therefore, possible to characterize and quantify the range of color variation of wet front at different *M*. The measurement steps are as follows: (1) A non-contact optical system (consisting of a Canon digital camera, camera mount, a digital scale, and photo booth) was used to record the MTPs gridded images on the various parts of the experimental board during the drying process when the $\overline{M}$ was 10%, 20%, 30%, 40%, 50%, and 60%. (2) The visible dry and wet zones present on the MTP under different $\overline{M}$ conditions were extracted using MATLAB 2018a for the *L*, *a*, and *b* values of pith, near-heart, tangential earlywood, tangential latewood, radial earlywood, and radial latewood and analyzed according to the *L*, *a*, and *b* standard colorimetric system (ISO 7724 standard). The color difference (Δ*E*) variation of the wet front was determined, which, in turn, defined the wet front of the wood in terms of according to the color difference, which was calculated according to Eq. (1) (Song et al. 2022).

$$\Delta E = \sqrt{\left(L_d - L_w\right)^2 + \left(a_d - a_w\right)^2 + \left(b_d - b_w\right)^2} \tag{1}$$

where *L*, *a*, and *b* parameters are luminance values *L*, redness–greenness color coordinate values *a*, and yellowness–blueness color coordinate values *b*, *d* with indexes: *d* indicates the corresponding values of the wood dry zone, and *w* indicates the corresponding values of the wood wet zone (the values of *L*, *a*, *b*, and Δ*E* can be found in "Dynamic changes in gloss and color values at various locations during drying" section).

Results and discussion

## Visible dynamic changes in 3D distribution of wood moisture during drying

The visible, dynamic changes of 3D moisture distributions of square poplar lumber during drying are shown in Fig. 2. Throughout the drying process, the $\overline{M}$ of the poplar boards was reduced from 60 to 10%. Its *M* distributions along the longitudinal, tangential, and radial directions were not symmetrically distributed, while there were irregular local *M* aggregation areas, whose area decreased along the growth rings of earlywood and latewood. At the early drying stage, the highest area of moisture distributions for the eight *MTP*s of Y-MC-60 sawing was at 2/6 and 5/6 from left to right along the tangential direction and 2/5–4/5 in the radial direction, with a minimum average *M* value of 56.7%. On the contrary, the *M* was lower in the heartwood position, with a maximum mean value of 45.6% (Fig. 2a). Throughout
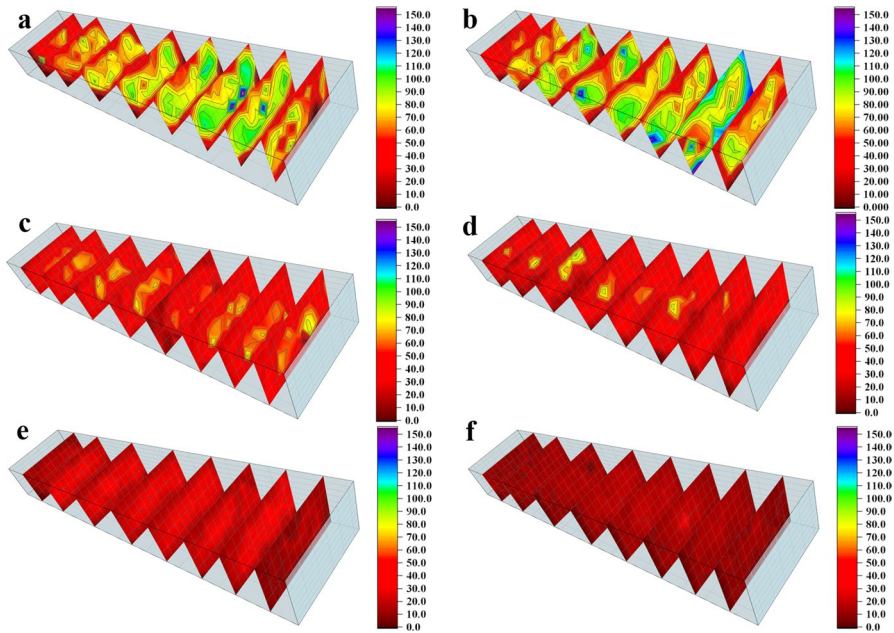
Fig. 2 Three-dimensional visual dynamic variation of poplar experimental boards moisture during the drying process. **a–f** 3D moisture distributions of experimental boards when the $\overline{M}$ is 60%, 50%, 40%, 30%, 20%, and 10%, respectively

the early drying process, M migration is from the high (at both ends of the radial direction) to the low M region (environment and heartwood region) by diffusion, as shown in Fig. 2b–d. When the exchange of water molecules between the high M areas and the low M areas reaches an equilibrium point, sapwood becomes the low M concentration area at the middle drying stage. When the heartwood M of Y-MC-40 became the highest, it ranged from 38.2 to 58.1%, indicating a board $\overline{M}$ between 40 and 50%, the point of maximum heartwood moisture may occur (Fig. 2c). Subsequently, the moisture migration changed to water migration from the heartwood (high M area) to the sapwood (low M area), as shown in Fig. 2d–f. When $M < 30\%$, the moisture distributions in the longitudinal direction tended to be homogeneous, with a deviation of 1.39–3.43%.

As shown in Fig. 3, the moisture migration pattern of the experimental pine lumber was more pronounced during drying, with asymmetric M evaporation along the longitudinal direction. The area of the highest M values in the thickness cross-section of S-MC-60, S-MC-50, and S-MC-40 migrated from the sides toward the middle. When the board $\overline{M}$ was above 30%, the M_i values showed lower values for heartwood (29.4–33.4%) than for sapwood. As the pine $\overline{M}$ decreased from 60 to 40%, the trend in the heartwood $\overline{M}$ values was initially 29.4% and then slowly increased to 36.8% after that decreasing to 33.4%. The heartwood of S-MC-30 was centrally located, and its M in the longitudinal direction and the eight MTPs remained asymmetrically distributed from left to right at 30.6–25.7%, with the same internal moisture migration along the earlywood and latewood growth rings. Meanwhile,
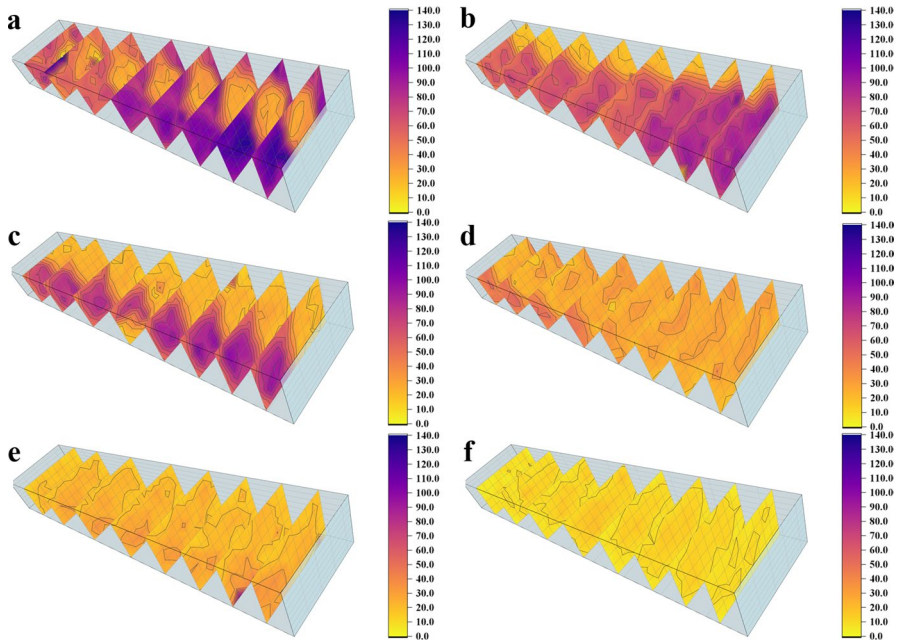
Fig. 3 Three-dimensional visual dynamic variation of camphor pine experimental boards moisture during the drying process. **a–f** 3D M distributions of experimental boards when the $\overline{M}$ is 60%, 50%, 40%, 30%, 20%, and 10%, respectively

Fig. 3a–f shows a clear M transition zone in the middle of the high and low concentration regions $\underline{M}$, and the highest value of M in this transition zone was 40–48.4% when the board $\overline{M}$ range was 40–50%. When $M < 30\%$, the M distribution in the longitudinal direction tended to be homogeneous, with a deviation of 0.98–1.6%.

Two-dimensional and 3D M differences in wood during drying

Generally, the wood drying term "deviation of M on thickness" is the inspection index of drying quality, and the center and surface M difference in the direction of wood MTP thickness (radial direction) shall prevail. However, the tangential direction M extreme difference value (TMCEV) also had an important influence on the production of moisture profiles due to the large M gradients within the wood. As shown in Fig. 4, the Y-axis was the position corresponding to MTPs under different $\overline{M}$ of experimental boards conditions, and the X-axis indicated the corresponding position in the radial direction with the color difference TMCEV. The TMCEV of wood during drying was larger at 2/5 and 4/5 in the radial direction, and the maximum difference was 109% and 105.7% when the $\overline{M}$ of experimental board was 60%, respectively, and the TMCEV tended to be below 10% as the $\overline{M}$ dropped below 20%. As Chi et al. (2022) analyzed the strain in the thickness cross-section during drying, also when the M to 20%, the strain in the tangential direction no longer continues
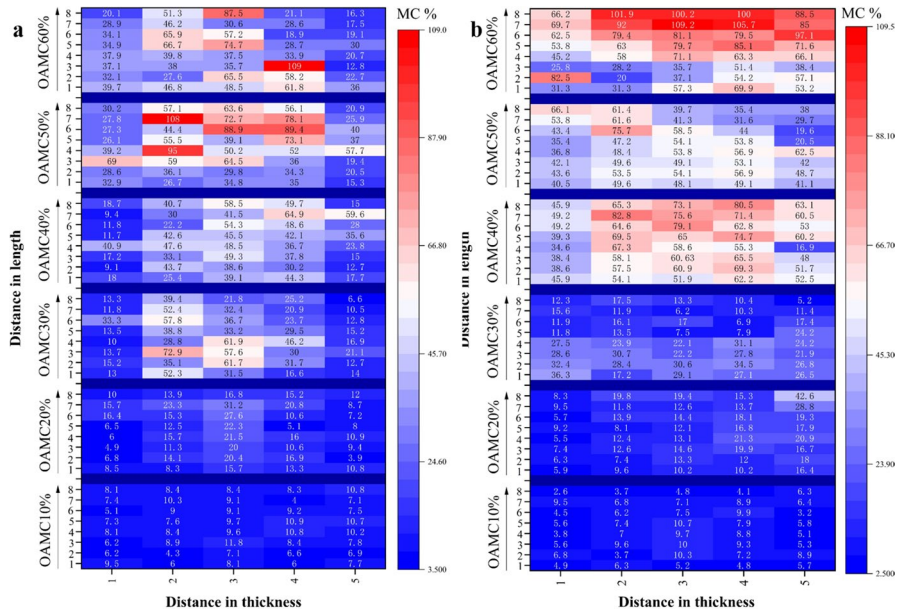
Fig. 4 TMCEV of MTP for each *M* condition of poplar (**a**) and pine (**b**) lumber

to increase; the larger *M* gradient with temperature gradient was the main factor causing the deformation of the wood, the development of stresses, and "wet lines." Meanwhile, the $\overline{M}$ variation of experimental boards (3D, as shown in Fig. 4) and the mean *M* variation of each *MTP* (2D, as shown in Tables 1 and 2) show *M* asymmetry along the longitudinal and radial directions. This phenomenon further proved the existence of non-Fickian behavior for water migration in wood during drying, and modeling should not be easily reduced to a 1/4 or 1/2 symmetric model. While the $\overline{M}$ of experimental boards decreased with drying time, the mean square difference between the mean *M* of moisture sections and $\overline{M}$ of experimental boards also decreased with drying time, and the mean square difference reached the minimum value of 1.6 and 1.3 when $\overline{M}$ was 10%, respectively.

Table 1 Difference between $\overline{M}$ and (two-dimensional) MTPs of poplar lumber

M%	Location								
	1	2	3	4	5	6	7	8	σ
60	12.00	− 11.21	− 15.73	− 7.92	− 1.59	1.09	4.70	18.66	10.92
50	19.05	1.46	− 9.42	3.05	− 7.59	− 7.54	− 2.00	2.99	8.59
40	− 0.60	0.45	0.67	2.06	− 8.27	2.04	1.46	4.07	3.47
30	1.60	2.03	− 2.84	− 2.34	− 0.68	− 2.70	1.04	3.88	2.35
20	5.65	− 2.06	− 2.43	− 2.21	− 2.89	− 0.69	− 3.44	8.06	4.07
10	1.71	0.87	− 0.34	− 1.95	− 2.12	− 1.17	0.37	2.63	1.60

Table 2 Difference between $\overline{M}$ and (two-dimensional) MTPs of pine lumber

M%	Location								
	1	2	3	4	5	6	7	8	σ
60	12.57	13.49	14.46	−3.02	−4.83	−4.03	−15.95	−12.68	11.25
50	12.35	9.21	7.27	4.46	4.16	−7.87	−13.19	−16.11	10.14
40	1.95	−0.75	0.31	10.85	−0.29	−3.84	−4.22	−2.92	4.52
30	−2.25	−2.25	−1.92	−2.25	1.51	2.01	2.52	2.63	2.19
20	4.42	0.48	−0.27	−0.74	−0.52	1.31	−2.5	−2.17	2.04
10	2.26	−0.40	−0.23	−2.45	0.30	−0.92	−0.27	1.37	1.33

## Dynamic changes in the dry and wet zones of wood during drying

Figure 5 shows that the grayscale images of the MTPs of poplar and camphor pine at each M, with the dark colors, represent the M contours of the wood, the "visible wet zone," and the wet front. When the M values of poplar and pine MTPs were 75.9% and 78.1%, respectively, at the beginning of drying, a wet front was observed to be present, and poplar MTPs showed discontinuous fan-shaped moisture areas in near-heartwood and sapwood, and also, there were scattered moisture areas, and likewise, wet front of camphor pine appeared between different growth rings. As the M decreased, wet front localization became more significant, with the wet front located at the sapwood growth whorl at approximately 1/10–2/10 of the MTP when M was 30.6%. As shown in Fig. 5a and b, the wet front was contoured by the early-wood and latewood growth rings, which gradually became smaller along the tangential direction. Combined with Figs. 2 and 3, the effect of wood 3D structure on the wet front showed tangential > radial > longitudinal direction. The M of poplar and camphor pine MTPs at the disappearance of wet front ranged from 14.26 to 19.7% and 20.4 to 22.5%, respectively.

Figures 6 and 7 represent the M box line diagrams corresponding to the wood units in the dry and wet zones visible for each $\overline{M}$ of experimental board condition during drying for poplar and camphor pine, respectively. The results showed that the M value did not bound the M corresponding to the visible dry and wet zones. We hypothesize that there are two reasons for this. Firstly, perhaps, one should not consider M as a state reached a certain water content (i.e., a certain point), but rather as Engelund et al. (2013) considered it as M when the entry of new water molecules into the cell wall leads to the breaking of intra- and intermolecular hydrogen bonds in the wood cell polymer, where the new molecules are accommodated in the cell wall without breaking further polymer H-bonds, and does not represent a specific water value. Secondly, if M_{fsp} is considered a state that reaches a particular M (i.e., a certain point), but M at the microscopic level is not detected by the weighing method, there may be an arrangement of aggregates of cells in macroscopic wood units. As shown in Fig. 8, the wet front on the surface was composed of cells in the saturated state of the fiber, but there were a large number of cell aggregates in the unsaturated state hidden underneath the surface, and the true average M of the
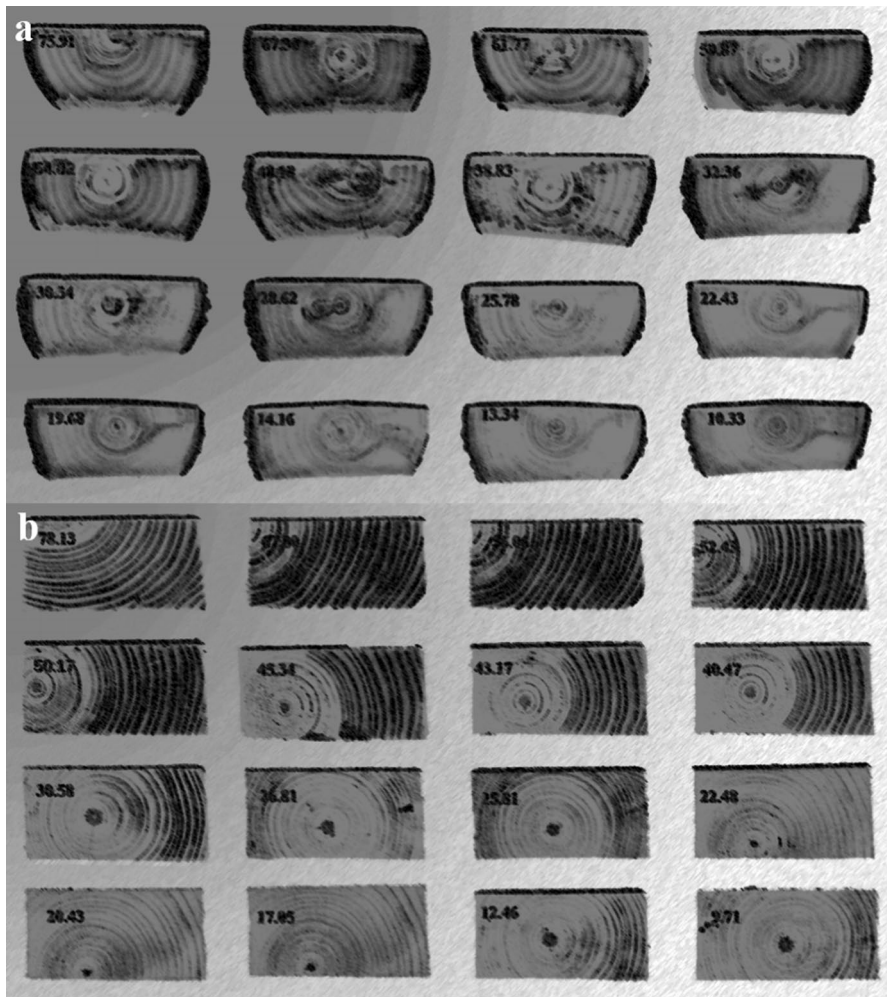
Fig. 5 The process of moisture visualization dynamics of poplar (**a**) and pine (**b**) TR sections

visible wet zone was less than the value corresponding to the M_{fsp} at this time. Conversely, the actual average M of the visible dry zone was larger than the value corresponding to the M_{fsp}, so the wet front needed to be defined more closely, as detailed in "Dynamic changes in gloss and color values at various locations during drying" section. Figures 6 and 7 show that when the M was 30%, it appeared that the visible dry zone ranges > visible wet zone range when the wet front disappeared, and its threshold should be somewhere under $M < 30\%$. As shown in Figs. 6 and 7, the minimum values of the average difference between dry and wet zones on poplar and camphor pine MTPs were 18.4% and 14.2%, respectively, when the wood M was 30%. The wet front can be used as a criterion to prove excessive local M deviation of wood in the middle and late stages of drying ($14.16\% < M < 30\%$).
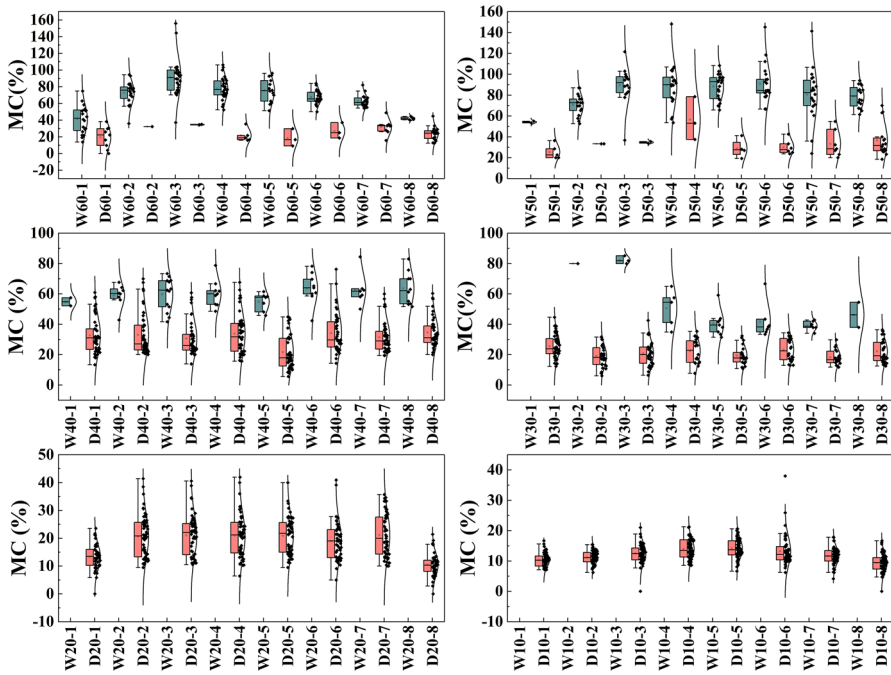
Fig. 6 Box line diagram of M distributions in dry and wet zones of poplar under each $\overline{M}\,\overline{M}$ condition. On the X-axis, W represents the wet zone, D represents the dry zone, and the values 60, 50, 40, 30, 20, and 10 correspond to the M of the samples, which is 60%, 50%, 40%, 30%, 20%, and 10%, respectively. The numbers 1–8 denote the corresponding two-dimensional slice positions of the samples

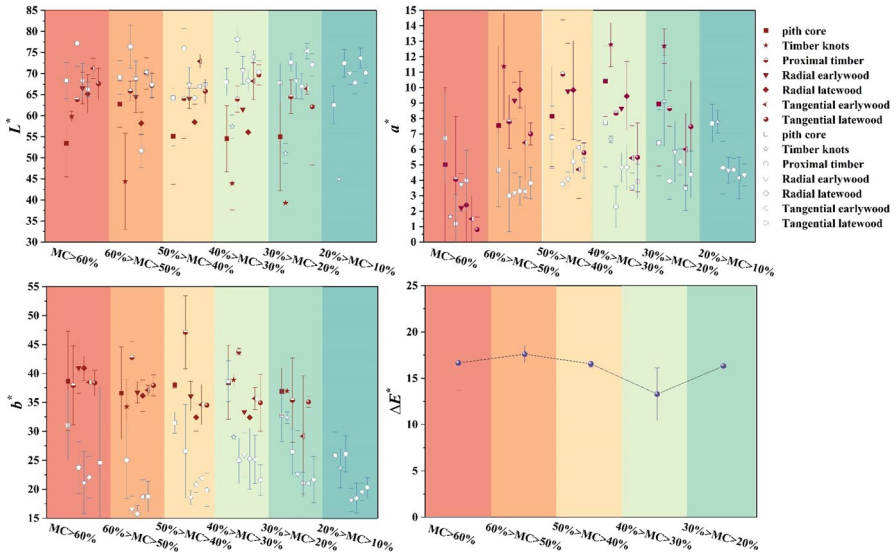## Dynamic changes in gloss and color values at various locations during drying

A wet front occurs because of a distinct color difference between the color of the free water-containing and critical areas of the wood cross-section, forming the visible area. As shown in Fig. 9, during the drying process, the gloss of the wood was changed with the position, the internal M. In this process, the highest L values were found in the dry zone of poplar near the heartwood, except for the nodes and pith, and the mean values of L for all parts of poplar at each M ranged from 72.5 to 78.2, with the $L_{Mfinal} > L_{Minitial}$. While the earlywood and latewood in the radial direction and tangential directions of camphor pine were not affected by yellowing during the drying process, the a and b values decreased as M decreased and L values increased (Fig. 10, the mean values of a and b for all parts of poplar at each M ranged from 0.81 to 12.78 and 15.77 to 47.11, respectively). Given, L, a, and b values were extracted and calculated separately for earlywood and latewood (R and T), wet and dry zones in the near-heartwood region for each M stage of wood during the drying process using MATLAB 2018a. According to the L, a, and b standard chromaticity system (ISO 7724 standard), it was possible to obtain
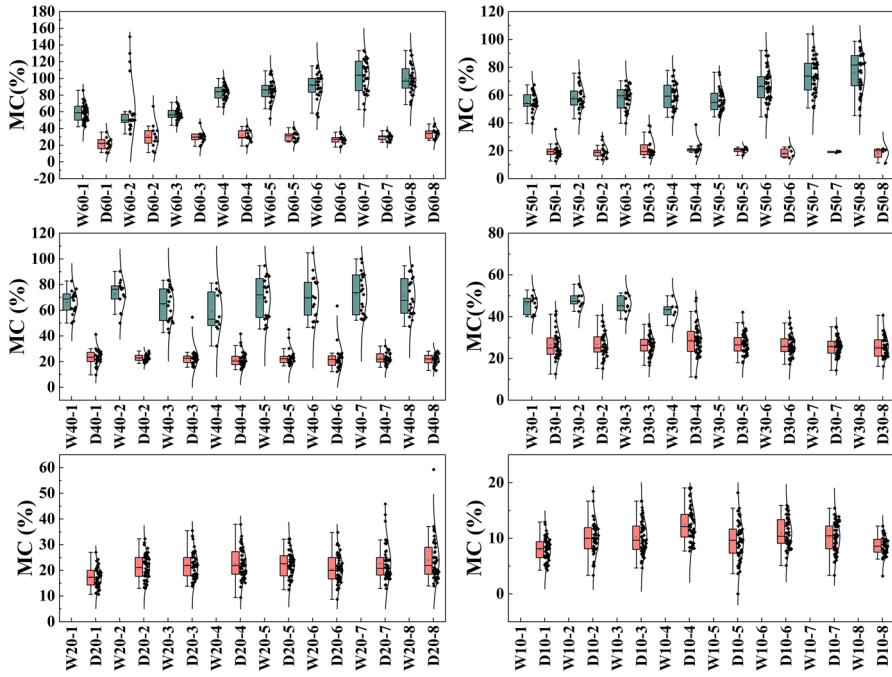
Fig. 7 Box line diagram of M distributions in dry and wet zones of camphor pine under each $\overline{M}$ condition. On the *X*-axis, *W* represents the wet zone, *D* represents the dry zone, and the values 60, 50, 40, 30, 20, and 10 correspond to the M of the samples, which is 60%, 50%, 40%, 30%, 20%, and 10%, respectively. The numbers 1–8 denote the corresponding two-dimensional slice positions of the samples
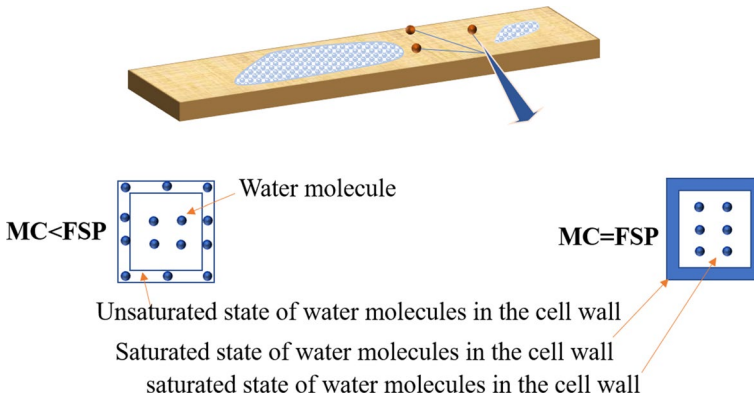
Fig. 8 Mechanism of intracellular water aggregation inside wood

Fig. 9 Changes in gloss and color values of poplar lumber. Where the shape of each symbol is solid for the wet zone and hollow for the dry zone
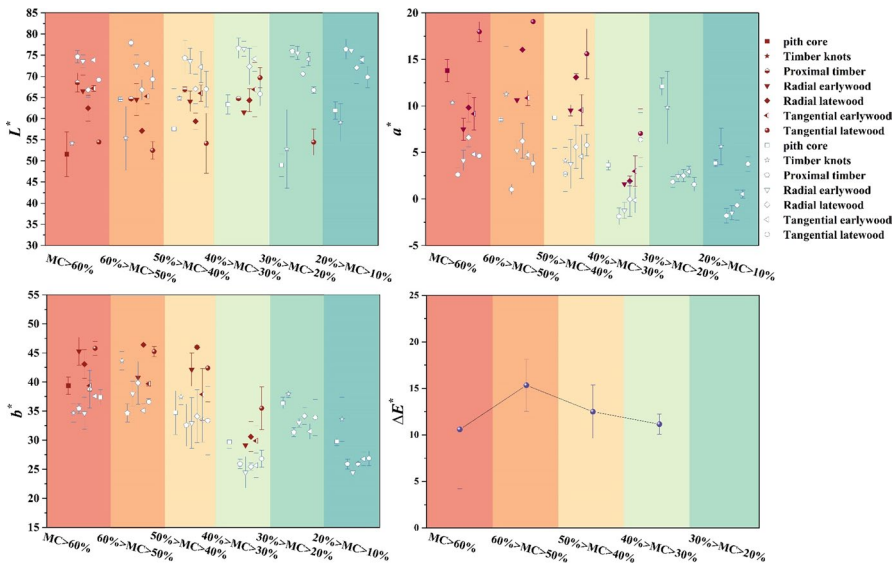
Fig. 10 Changes in gloss and color values of camphor pine lumber. Where the shape of each symbol is solid for the wet zone and hollow for the dry zone

an average (ΔE) range of color difference in the range of 10.6–17.6 for both kinds of woods with wet front (Figs. 9 and 10).

In summary, there are no absolute wet and dry zones inside hardwoods, while there are distinct wet and dry zones in softwoods. When T and H are constant, the reasons for the appearance and disappearance of the wet front may be the following two points. (1) Wood has a large amount of internal M, and its internal and external drying rates are different, resulting in a M gradient or M concentration difference; when higher than a specific M gradient wet front appears, and vice versa disappears. (2) The unique biological properties of wood caused variable porosity in the region of the growth rings of earlywood and latewood in the tangential and radial directions. The local variable porosity changed the positive relationship between the overall internal water concentration and the wood's diffusion coefficient compared to the whole wood. It was easy to form a high concentration region of localized moisture accumulation near the growth rings, thus forming a region of water evaporation surface near the growth rings, which Turner et al. (2011) attributed this phenomenon to the non-Fickian behavior of wood moisture migration.

Conclusion

The results showed that:

(1) When the $\overline{M}$ of experimental boards was between 40 and 50%, the point of the highest value of moisture content became the heartwood, as the high moisture region in the tangential direction reached an equilibrium point with the low moisture region of the heartwood, when the low moisture region became the sapwood and external environment of the wood.
(2) There are non-Fickian behaviors for water migration in wood, the wet front was contoured by the growth whorl of earlywood and latewood and became progressively smaller along the tangential direction, and the influence of wood 3D structure on the wet front was tangential > radial > longitudinal direction, the M of poplar and camphor pine MTPs at the disappearance of wet front ranged from 14.2–19.7% to 20.4–22.5%, respectively.
(3) TMCEV of wood during drying was larger at 2/5 and 4/5 in the R direction.
(4) The M corresponding to the visible dry and wet zones may not be absolutely bounded by the M_{fsp} value, and the average range of the color difference ΔE was 10.59–17.61 when wet front occurs for both wood pieces. It is necessary to clarify that the conclusions apply to these two tree species and that subsequent research needs to find suitable ways to improve further the accuracy of data collection and visualization and further validation for other tree species.

Finally, the disappearance of the wet front means that the late stage of drying is reached, while the modeling of thermal mass transfer during wood drying should be carefully simplified and not homogenize in the 3D wood model.

Author contributions XC helped in funding acquisition, formal analysis, conceptualization, methodology, investigation, data curation, visualization, writing—original draft, project administration, and supervision. SA contributed to writing—review and editing, conceptualization, and supervision. ST worked in investigation, methodology, and resources. ZR and XS worked in resources and validation. WC and GH worked in project administration and supervision. Since this experiment cannot be intermittent, we need to live next to the equipment. Special thanks to BX and ML for delivering meals three times a day during the whole experiment and participating in the measurement of the experimental data. Thanks to Professor Xie for his guidance on this paper.

Declarations

Conflict of interest The authors declare no conflict of interest.

References

Adamski R, Pakowski Z (2013) Identification of effective diffusivities in anisotropic material of pine wood during drying with superheated steam. Dry Technol 31(3):264–268

Arends T, Pel L, Smeulders D (2018a) Moisture penetration in oak during sinusoidal humidity fluctuations studied by NMR. Constr Build Mater 166:196–203

Arends T, Barakat AJ, Pel L (2018b) Moisture transport in pine wood during one-sided heating studied by NMR. Exp Therm Fluid Sci 99:259–271

Avramidis S, Hatzikiriakos SG, Siau JF (1994) An irreversible thermodynamics model for unsteady-state nonisothermal moisture diffusion in wood. Wood Sci Technol 28(5):349–358

Cai C, Javed MA, Komulainen S et al (2020) Effect of natural weathering on water absorption and pore size distribution in thermally modified wood determined by nuclear magnetic resonance. Cellulose 27(8):4235–4247

Chen Z, Zhuo H, Hu Y et al (2020) Wood-derived lightweight and elastic carbon aerogel for pressure sensing and energy storage. Adv Funct Mater 30(17):1910292

Chetpattananondh P, Thongpull K, Chetpattananondh K (2017) Interdigital capacitance sensing of moisture content in rubber wood. Comput Electron Agric 142:545–551

Chi X, Xu J, Han G et al (2020) Selection of cross-seasonal heat collection/storage media for wood solar drying. Dry Technol 38(16):2172–2181

Chi X, Tang S, Du X et al (2022) Effects of air-assisted solar drying on poplar lumber drying processes in sub frigid zone regions. Dry Technol 40(16):3580–3590

Chiniforush AA, Valipour H, Akbarnezhad A (2019) Water vapor diffusivity of engineered wood: effect of temperature and moisture content. Constr Build Mater 224:1040–1055

Droin-Josserand A, Taverdet JL, Vergnaud JM (1989) Modelling of moisture absorption within a section of parallelepipedic sample of wood by considering longitudinal and transversal diffusion. Holzforschung 43(5):297–302

Engelund ET, Thygesen LG, Svensson S et al (2013) A critical discussion of the physics of wood–water interactions. Wood Sci Technol 47(1):141–161

Fredriksson M, Thybring EE, Zelinka SL (2021) Artifacts in electrical measurements on wood caused by non-uniform moisture distributions. Holzforschung 75(6):517–525

Gambarelli S, Ožbolt J (2021) 3D hygro-mechanical meso-scale model for wood. Constr Build Mater 311:125283

Gan W, Wang Y, Xiao S et al (2021) Magnetically driven 3D cellulose film for improved energy efficiency in solar evaporation. ACS Appl Mater Interfaces 13(6):7756–7765

Gilania MS, Abbasion S, Lehmann E et al (2014) Neutron imaging of moisture displacement due to steep temperature gradients in hardwood. Int J Therm Sci 81:1–12

Guan H, Cheng Z, Wang X (2018) Highly compressible wood sponges with a spring-like lamellar structure as effective and reusable oil absorbents. ACS Nano 12(10):10365–10373

Hao X, Yu C, Zhang G et al (2020) Modeling moisture and heat transfer during superheated steam wood drying considering potential evaporation interface migration. Dry Technol 38(15):2055–2066

He Z, Qian J, Qu L et al (2019) Simulation of moisture transfer during wood vacuum drying. Results Phys 12:1299–1303

He S, Chen C, Li T et al (2020) An energy-efficient, wood-derived structural material enabled by pore structure engineering towards building efficiency. Small Methods 4(1):1900747

Kandala CV, Holser R, Settaluri V et al (2016) Capacitance sensing of moisture content in fuel wood chips. IEEE Sens J 16(11):4509–4514

Li W, den Bulcke JV, Windt ID et al (2013) Combining electrical resistance and 3-D X-ray computed tomography for moisture distribution measurements in wood products exposed in dynamic moisture conditions. Build Environ 67:250–259

Lingayat AB, Chandramohan VP, Raju VRK et al (2020) A review on indirect type solar dryers for agricultural crops—dryer setup, its performance, energy storage and important highlights. Appl Energy 258:114005

Lu Y, Fan D, Shen Z et al (2022) Design and performance boost of a MOF-functionalized-wood solar evaporator through tuning the hydrogen–bonding interactions. Nano Energy 95:107016

Mikac U, Serša I, Zupanc MŽ et al (2018) Application of MR microscopy for research in wood science. Microporous Mesoporous Mater 269:51–55

Oh GH, Kim HS, Park DW et al (2020) In-situ monitoring of moisture diffusion process for wood with terahertz time-domain spectroscopy. Opt Laser Eng 128:106036

Oliveira F, Candian M, Lucchette FF et al (2005) A technical note on the relationship between ultrasonic velocity and moisture content of Brazilian hardwood (*Goupia glabra*). Build Environ 40(2):297–300

Pan P, McDonald TP, Via BK et al (2016) Predicting moisture content of chipped pine samples with a multi-electrode capacitance sensor. Biosyst Eng 145:1–9

Purba CYC, Viguier J, Denaud L et al (2020) Contactless moisture content measurement on green veneer based on laser light scattering patterns. Wood Sci Technol 54(4):891–906

Redman AL, Bailleres H, Gilbert BP et al (2018) Finite element analysis of stress-related degrade during drying of *Corymbia citriodora* and *Eucalyptus obliqua*. Wood Sci Technol 52(1):67–89

Song X, Han G, Jiang K et al (2022) Effect of wood microstructure and hygroscopicity on the drying characteristics of waterborne wood coating. Wood Sci Technol 56(3):743–758

Turner I, Ilic M, Perre P (2011) Modelling non-fickian behavior in the cell walls of wood using a fractional-in-space diffusion equation. Dry Technol 29(16):1932–1940

Watanabe K, Saito Y, Avramidis S et al (2008) Non-destructive measurement of moisture distribution in wood during drying using digital X-ray microscopy. Dry Technol 26(5):590–595

Zhao J, Cai Y (2017) A comprehensive mathematical model of heat and moisture transfer for wood convective drying. Holzforschung 71(5):425–435